Acta Cryst. (1982). A**38**, 522–529

Short-Range Ordering and Ferromagnetic Properties of Disordered Au_4Mn Alloy

BY H. SUZUKI AND J. HARADA

Department of Applied Physics, Nagoya University, Nagoya, Japan

AND T. NAKASHIMA* AND K. ADACHI

Department of Iron and Steel Engineering, Nagoya University, Nagoya, Japan

(*Received* 16 *December* 1981; *accepted* 5 *March* 1982)

Abstract

The short-range-order (SRO) parameters of disordered Au_4Mn alloy were determined from an analysis of the X-ray diffuse scattering with the use of Borie & Sparks [*Acta Cryst.* (1971), A**27**, 198–201] separation techniques. On the basis of the observed SRO parameters the local Mn atom arrangement in the f.c.c. lattice was constructed using a computer simulation method. The Mn atoms in the SRO state were found to form a three-dimensional irregular network which is linked mainly by linear chain segments along the [100] directions and also with nearest-neighbour relations. The Mn atom arrangement is the first example to show the structure expected from a random spin system with a concentration gradient. The ferromagnetic properties of this state can be well understood on the basis of the structure.

1. Introduction

The binary alloy Au_4Mn has a Ni_4Mo type structure below the critical temperature of 693 K. Between 693 and 753 K, a mixture of the ordered Au_3Mn (α'' phase) and a disordered phase exists. A single disordered f.c.c. structure is seen above 753 K (Köster & Hummel, 1964). This alloy has a peculiar order–disorder transition in which the superlattice reflections in the ordered state have no special relationship to the short-range-order (SRO) diffuse scattering of the disordered state. Both the ordered and the disordered alloy show ferromagnetism at low temperature indicating that the phase transitions are independent of the chemical order–disorder transition. The disordered ferromagnet which is of current physical interest is not yet understood on the basis of its structure.

The disordered structure above 753 K has been investigated by Nakashima, Mizuno, Ido, Sato, Mitani & Adachi (1977) and very recently by Fürnrohr, Epperson & Gerold (1980): hereafter referred to as NMISMA and FEG, respectively. By paying attention to the fact that the Mn atom has a negative scattering length for neutrons, NMISMA observed SRO diffuse scattering using neutron diffraction methods and obtained the Warren–Cowley short-range-order parameters. They also determined the atomic pair interaction potentials on the basis of the Clapp–Moss formalism (Clapp & Moss, 1966, 1968*a*,*b*). It is pointed out in their study that higher-order SRO parameters may be required in the understanding of the local atomic arrangements of the disordered state. But their measurements do not satisfactorily reproduce the local atomic arrangement because the separation of the SRO diffuse scattering from the size modulation effect and thermal diffuse scattering plus Huang scattering has not been properly made.

FEG evaluated the SRO parameters by using the Borie–Sparks separation method for X-ray diffuse scattering (Borie & Sparks, 1971). They also studied the effect of various heat treatments on the local atomic arrangement, particularly on the Mn atoms, by making use of a computer simulation method developed by Gehlen & Cohen (1965). They showed that the atomic arrangement is characterized by the development of Mn chains along the cubic axes. In addition to this, they confirmed that the arrangement does not approach the ordered state even with increasing annealing time. In this computer simulation, however, only six SRO parameters were adjusted to fit the observed values, although medium-range-order parameters are known to be significant, as pointed out by NMISMA. Despite such extensive structural studies of the disordered state, it is not clear exactly what relationship exists between the atomic arrangements in ordered and disordered states.

Since the initial neutron diffraction study by NMISMA, we have extended the study by using X-ray diffuse scattering techniques to obtain more accurate information about the local atomic arrangement of this Au_4Mn alloy. Our study indicates that the Mn atoms in the SRO state form a three-dimensional irregular

* Present address: IBM Japan Ltd, Districtt Hokkaido, Sapporo, Japan.

0567-7394/82/040522-08$01.00

network which is linked mainly by linear chain segments along the [100] directions and also with nearest-neighbour relations in the f.c.c. lattice. It was also found that the existence of Mn atom pairs with nearest-neighbour relations plays an important role in this ferromagnet. As nearest-neighbour interactions have antiferro coupling, the antiferromagnetic component is not negligible. In this paper we show the detailed atomic arrangement of the SRO state and discuss the ferromagnetic properties of this state on the basis of the structure.

The X-ray diffuse scattering measurements were made using a rotation-anode high-power X-ray generator developed at the HIX Laboratory, Nagoya University, for easy measurements of weak diffuse scattering.

2. Experimental procedures

2.1. *Sample preparation*

The single-crystal sample of Au_4Mn, which had been used in the study of NMISMA, was again employed in the present study by forming it into a disk shape of 8 mm diameter × 0·8 mm thickness, the top surface being the (210) plane. The original crystal was prepared by the Bridgman method with a temperature gradient of 40 K cm^{-1} and at a cooling rate of 2·5–3·0 K h^{-1} through the melting point 1293 K as indicated in the previous paper (NMISMA). The sample was then continually homogenized at 1223 K for one week and then annealed at 773 K for 2 d and quenched in iced water. Analysis of Laue and Debye photographs confirmed that the sample had the disordered f.c.c. structure with lattice parameters of 4·0630 (5) Å, and manganese composition of 20·3 (3) at.% Mn from Vegard's law.

2.2. *Instrumentation*

A four-circle diffractometer, Rigaku AFC-5, controlled by a minicomputer, Pnafacom U-100, was connected to a high-power X-ray generator, Rigaku RU-1500, in the HIX Laboratory, Nagoya University. Maximum power attained by the generator is 90 kV (60 kV, 1500 mA) with a focus area of 1 × 10 mm for the Cu target. Fig. 1 shows the schematic arrangement of the instrument. Cu $K\alpha$ radiation was made monochromatic by a plate-like pyrolytic graphite monochromator. The distance between the X-ray source and the monochromator was 350 mm. The incident beam was passed through a Co film with 95% transparency. Fluorescence radiation from the Co film was used as a monitor of the incident beam fluctuations. Balanced filters of Ni–Co were placed just after the film, and the $\lambda/2$ contributions were eliminated by subtracting the intensity through the Co filter from that through the Ni filter. The X-ray beam was collimated with a 1 mm^{φ} slit. The size of the beam section on the sample by the collimator was 1·1 mm^{φ}. The horizontal and vertical divergences were 0·37 and 0·33°, respectively. A Pb baffle was set to prevent air scattering. The scattered X-rays from the sample were detected through the receiving path of dimensions 5^{φ} × 75 mm, by a main counter with receiving slits of 1 × 1°.

2.3. *Measurement programs*

We developed a control program for the measurement of diffuse scattering, the flow chart of which is shown in Fig. 2. In this program, four axes are driven to the destination angles calculated from the indices of the measurement region which is stored in a disk storage device. The diffuse scattering is then measured for each balanced filter until the monitor counts a fixed value. This method is advantageous in the case of fluctuations in the incident beam. The data obtained were stored on disk.

2.4. *Method of measurement*

The disk-shaped specimen was positioned on a goniometer head, so that its surface was at the centre of the diffractometer with its normal parallel to the φ rotation axis. The *UB* matrix was then determined from three sets of angles observed for the 200, 220, and 111 reflections.

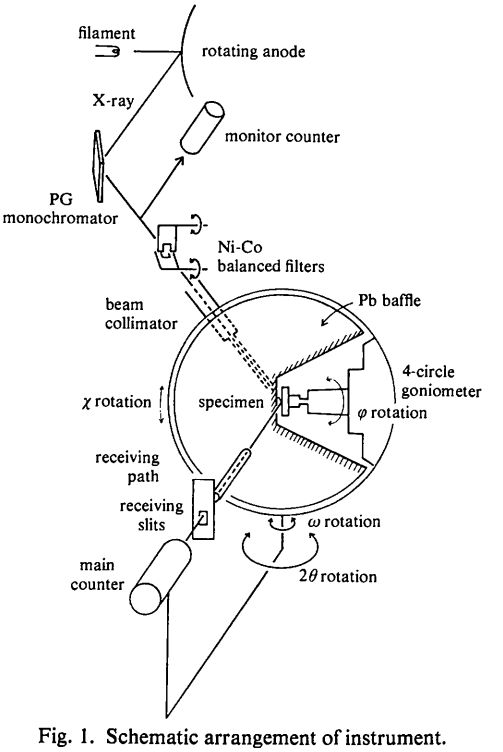

Fig. 1. Schematic arrangement of instrument.

The measurement of the diffuse scattering was carried out at 1483 points on a cubic grid over the volume in reciprocal space in Fig. 3 with an interval of $\Delta h_i = 0{\cdot}1$ (h_i represents the coordinates in reciprocal space). Each measurement was made with the monitor set on 120 000 counts, which corresponded to 15 s at the operating conditions of 52·5 kV, 1200 mA. In order to ensure the reliability of the observed data, the conspicuous diffuse scattering at $(1,\frac{1}{2},0)$ was measured after every 25 measurements as a reference. The fluctuation of the intensity at this reference point was within $\pm 3\%$ through the whole experiment.

3. Results and analysis

3.1. *Observed intensities*

Observed intensities, I(obs), were converted to absolute intensities I_{eu}/N, in electron units, by comparing the intensities from a polystyrene, C_8H_8, sample. The formula used in this conversion is

$$\frac{I_{eu}}{N} = \frac{[I(\text{obs}) - I(B)]}{[I'(\text{obs}) - I(B)]} \frac{M}{M'} \frac{(\mu/\rho)}{(\mu/\rho)'} \frac{(PF)'}{(PF)} \left(\frac{I_{eu}}{M}\right)' \frac{1}{0{\cdot}95}. \quad (1)$$

$(I_{eu}/M)'$ is the calculated intensity per molecule from C_8H_8 (64·62). I(obs) and I'(obs) are the measured intensities from the specimen and C_8H_8, respectively. $I(B)$ is the background intensity; (PF) and $(PF)'$ are the polarization factors for the sample and C_8H_8, respectively. M and M' are the molecular weight of AuMn (168·59) and C_8H_8 (104·15), respectively, and 0·95 is the correction factor due to double scattering in C_8H_8. The mass absorption coefficients for the sample and C_8H_8 are $(\mu/\rho) = 213{\cdot}0$ and $(\mu/\rho)' = 4{\cdot}28$, respectively. After conversion to absolute units Compton scattering contributions were subtracted, and the results were divided by $m_A m_B (f_A - f_B)^2$, where m_A and f_A are the concentration and atom form factor, respectively, for the A-type atom.

The diffuse scattering distribution

$$I^D(\text{obs}) = I_{eu}/N . m_A m_B (f_A - f_B)^2,$$

for the $(h_1,h_2,0)$ reciprocal-lattice plane is shown in Fig. 4 in which three diffuse peaks at $(1,\frac{1}{4},0)$, $(1,\frac{1}{2},0)$, $(1,\frac{3}{4},0)$ and their equivalence in the reciprocal space are clearly seen. The results are in good agreement with the previous observations given by NMISMA and FEG. The three diffuse peaks do not coincide with specific superlattice reflection positions of Ni_4Mo-type structure, which is expected to appear below the phase transition temperature.

3.2. *Borie–Sparks separation*

In general, the observed diffuse scattering intensities converted to electron units are composed of four terms;

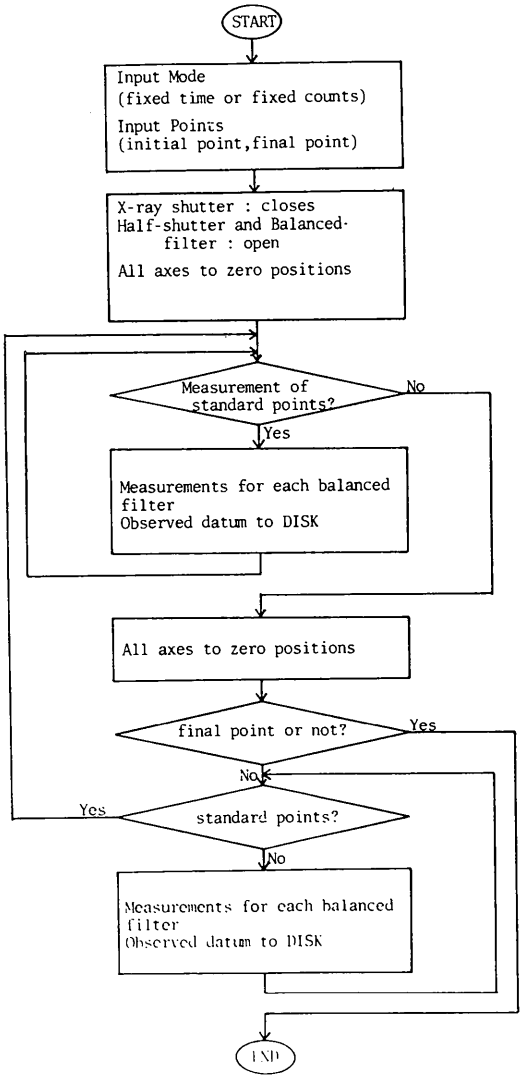

Fig. 2. Flow chart of control program for the measurement of diffuse scattering.

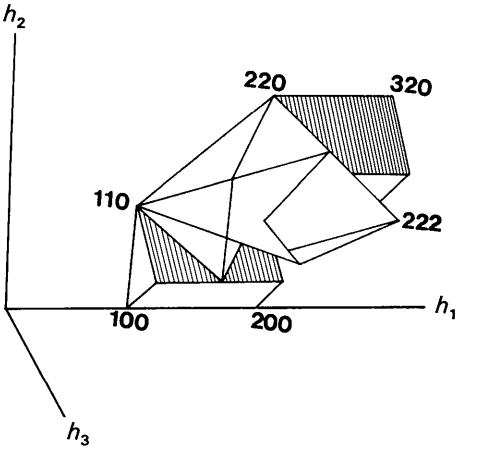

Fig. 3. Volume of reciprocal space over which diffuse scattering measurement was taken.

contribution from SRO diffuse scattering I(SRO), size effect modulation I(SE) and contribution from Huang and thermal diffuse scattering. The last two terms are described by I(TDS + H), because it is usually not possible to separate them. If the Borie–Sparks (1971) technique is applied to analyse the observed intensity distribution, the three terms can be separated from measured intensities on the basis that each term modulates differently in reciprocal space.

By applying this separation technique to the present data, I(SRO), I(SE) and I(TDS + H) were obtained. I(SRO) separated from the other diffuse scattering is shown in Fig. 5 for the $(h_1,h_2,0)$ plane. It is recognized from Fig. 5 that there exist appreciable intensities around the two Bragg points 200 and 220, in addition to the expected three peaks along the [100] directions from the 110 reciprocal-lattice point. Such extra intensities around the Bragg points conflict with the concept of short-range ordering. It is conceivable, however, that there are several inevitable contaminations around Bragg reflections due to the mosaic nature of the monochromator crystal and the sample. We, therefore, ignored the intensities near the Bragg peaks by regarding them as spurious scattering.

In view of the several assumptions on which the separation method is based, in order to see whether the Borie–Sparks separation technique has successfully analysed, diffuse intensities were reconstructed by synthesizing reversely each contribution obtained in a reduced zone and were compared with the observed intensities. Fig. 6 shows this comparison along the route from the 110 to the 310 points. The reproducibility is excellent as a whole, although I^D(cal) is slightly lower than I^D(obs) in regions of higher $h_1h_2h_3$ indices. This discrepancy is well understood as being due to the inherent deficiency of the Borie & Sparks method, as has been pointed out by several authors (Hayakawa, Bardhan & Cohen, 1975; Tibballs, 1974), since the diffuse scattering is assumed to be expressed

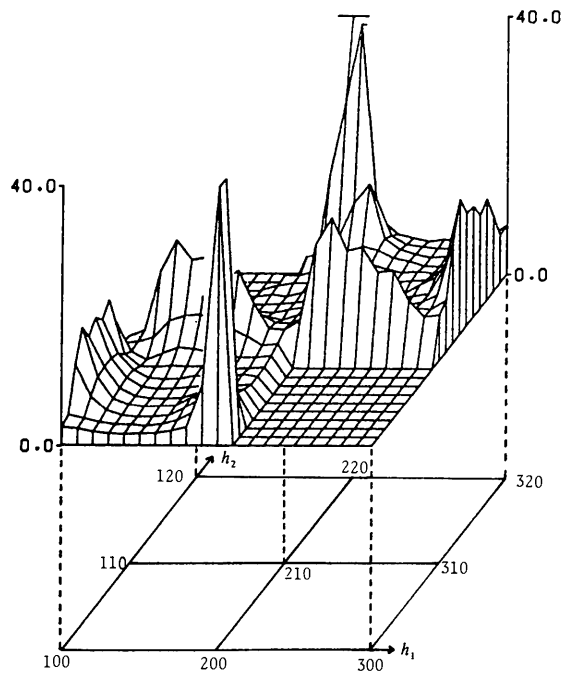

Fig. 4. Diffuse X-ray scattering distribution of the SRO state of Au_4Mn alloy for the (h_1h_20) reciprocal-lattice plane. The huge peaks around 200 and 220 are due to the tail of Bragg scattering.

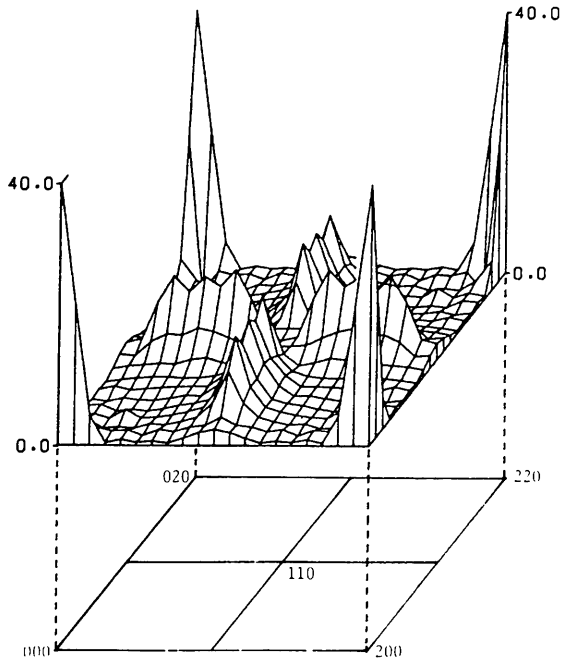

Fig. 5. The SRO diffuse scattering distribution around the 110 reciprocal-lattice point for the disordered Au_4Mn alloy. The peaks around each corner are due to the tail of Bragg scattering.

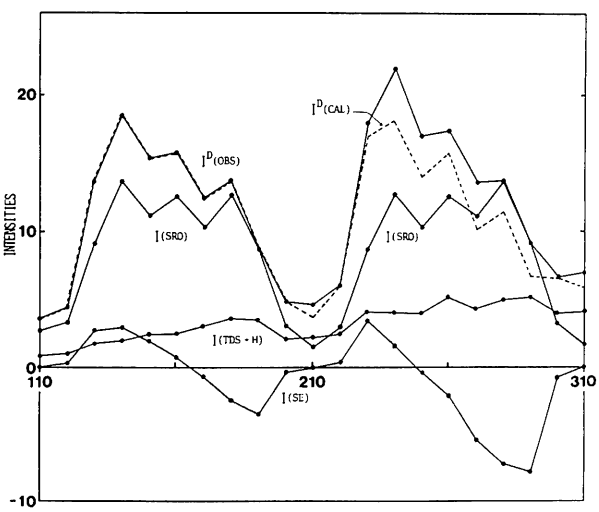

Fig. 6. The diffuse X-ray scattering synthesized from the three contributions of I(SRO), I(SE) and I(TDS + H) and those observed. Comparison is made along the route from the 110 to the 310 reciprocal-lattice points.

by up to quadratic terms and all higher-order terms are neglected in the expression of the exponential term. In addition, the ratios of $f_A/(f_A - f_B)$ and $f_B/(f_A - f_B)$ are taken to be constant over the whole volume of interest. In Au_4Mn alloy their modulations are estimated to be about 4 and 12% respectively, which are comparatively significant.

3.3. *Short-range-order parameters*

Three-dimensional Fourier transforms of the SRO diffuse intensities determined the SRO parameters, α_{lmn}. They are listed in Table 1 together with the results of NMISMA and FEG.

The present analysis gives a value of 1·07 for α_{000}, which is very close to the theoretically expected value of 1. Although α_{000} is close to 1, this does not necessarily prove that the measurement and the analysis are satisfactory. It may, however, be assumed that the present investigation is reliable.

The values of the α_{lmn} themselves are quite different from those of NMISMA, while the *lmn* dependence of SRO parameters is very similar. The numerical difference between the two results can therefore be interpreted as due to the fact that in NMISMA's experiment the measurements were not made on an absolute scale, which introduces several errors in the estimation of the SRO parameters. On the other hand,

Table 1. *Short-range-order parameters of disordered* Au_4Mn

Reliability of the parameters is given by comparing the observed $\alpha_{000} = 1{\cdot}07$ with the theoretically expected value $\alpha_{000} = 1$.

	Nakasima *et al.* (1977)	Fürnrohr *et al.* (1980)	Present work	Present work Simulation
0 0 0	1·000	1·060	1·076	
1 1 0	−0·078	−0·201	−0·168	−0·167
2 0 0	0·099	0·209	0·222	0·221
2 1 1	0·038	0·052	0·042	0·042
2 2 0	0·009	−0·005	0·014	0·014
3 1 0	0·053	−0·079	−0·087	−0·086
2 2 2	−0·082	−0·097	−0·128	−0·128
3 2 1	0·024	0·031	0·044	0·044
4 0 0	0·074	0·106	0·163	0·163
3 3 0	−0·036	−0·044	−0·064	−0·064
4 1 1	0·004	0·003	−0·000	0·000
4 2 0	0·010	0·009	0·016	0·016
3 3 2	0·015	0·011	0·007	0·008
4 2 2	−0·033	−0·032	−0·049	−0·049
4 3 1	0·004		0·006	0·006
5 1 0	−0·024		−0·056	−0·056
5 2 1	0·010		0·016	0·016
4 4 0	0·009		0·016	0·017
4 3 3	0·004		0·011	0·010
5 3 0	−0·017		−0·034	−0·034
4 4 2	−0·015		−0·018	−0·018
6 0 0	0·029		0·096	0·095

Table 1 (*cont.*)

	Nakasima *et al.* (1977)	Fürnrohr *et al.* (1980)	Present work	Present work Simulation
5 3 2	0·006		0·016	0·016
6 1 1	0·001		0·003	0·003
6 2 0	0·005		0·016	0·016
5 4 1	0·003		0·017	0·016
6 2 2	−0·010		−0·027	
6 3 1	0·001		−0·001	
4 4 4	−0·010		−0·031	
5 4 3	0·003		0·004	
5 5 0	−0·008		−0·039	
7 1 0	−0·008		−0·027	
6 4 0	0·003		0·019	
5 5 2	0·002		0·007	
6 3 3	0·000		−0·000	
7 2 1	0·002		0·022	
6 4 2	−0·005		−0·019	
7 3 0	−0·005		−0·026	
6 5 1	0·000		0·001	
7 3 2	0·001		−0·005	
8 0 0	0·016		0·042	
5 5 4	0·002		0·007	
7 4 1	0·002		0·004	
8 1 1	−0·006		−0·021	
6 4 4	−0·004		−0·013	
8 2 0	0·008		0·015	
6 5 3	0·000		0·006	
6 6 0	0·002		0·017	
8 2 2	0·003		−0·004	
7 4 3	0·001		0·007	
7 5 0	−0·002		−0·015	
8 3 1	−0·005		−0·001	
6 6 2	−0·001		0·000	
7 5 2	0·000		0·005	
8 4 0	0·004		0·014	
8 3 3	−0·003		−0·000	
9 1 0	−0·002		−0·028	
8 4 2	0·001		−0·010	
6 5 5	0·000		0·002	
7 6 1	0·000		−0·004	
9 2 1	0·000		0·016	
6 6 4	−0·001		−0·003	
7 5 4	0·001		0·001	
9 3 0	−0·001		−0·024	
8 5 1	−0·002		0·003	
7 6 3	0·000		−0·001	
9 3 2	0·000		0·001	
8 4 4	0·000		0·002	
7 7 0	−0·001		−0·010	
8 5 3	−0·002		−0·008	
9 4 1	0·000		0·001	
8 6 0	0·002		0·015	
10 0 0	0·002		0·061	
7 7 2	0·000		0·007	
10 1 1	−0·000		000·0	
8 6 2	0·001		0·000	
10 2 0	0·000		0·015	
9 4 3	0·000		0·003	
9 5 0	−0·000		−0·015	

the present results agree very well with the FEG study in spite of slight differences in the compositions of the samples used; 20 at.% Mn (this work) and 18 at.% Mn (FEG). Their paper presented 14 SRO parameters up to the 422 neighbour so that the α_{lmn} parameters with higher indices, which must play an essential role in such a complex SRO diffuse scattering distribution, cannot be compared with their results, but certainly no conspicuous differences are observed between the scattering distribution given by their paper and that shown in Fig. 5.

In Fig. 7 the α_{lmn} parameters are plotted against atomic distance, R_{lmn}. Among the α_{lmn} parameters, α_{200} (0·222), α_{400} (0·163), α_{600} (0·096), α_{800} (0·042), $\alpha_{10,0,0}$ (0·061) are positive and extremely large, indicating a very slow decrease with indices along the [100] direction and α_{110}, α_{310}, α_{510} and α_{710} have appreciable negative values. $\alpha_{10,0,0}$ has an even larger value. These results suggest that Mn atoms have a tendency to line up along the [100] direction up to 50th neighbours, occupying sequentially the second-neighbour atomic positions in the f.c.c. lattice as shown schematically in Fig. 8. This is probably due to their long-range interactions.

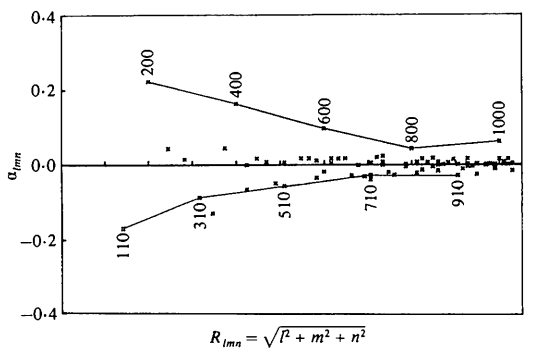

Fig. 7. Plot of the SRO parameters *vs* atomic distance R_{lmn} for the disordered Au_4Mn alloy.

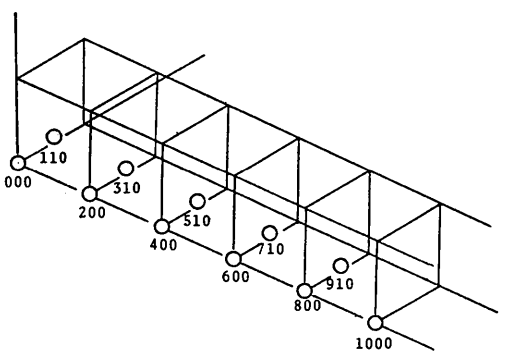

Fig. 8. A schematic representation of the Mn atom chain extending along the [100] direction in the f.c.c. lattice. The positions such as 200, 400, 600, and so on are probably occupied by a Mn atom, while those of 110, 310, 510, *etc.* by a different kind of Au atom, when the origin is occupied by a Mn atom.

3.4. *Computer simulation*

Gehlen & Cohen (1965) and Williams (1976) developed a computer simulation method simulating local atomic arrangements on the basis of observed α parameters. We examined such simulations for the Au_4Mn alloy by employing Williams's program modified by Hirabayashi, Koiwa, Yamaguchi & Kamata (1978). Initially two kinds of atoms in a given composition were distributed randomly on 10 × 10 × 10 f.c.c. unit cells, in which 4000 atomic sites were included, and then exchanges between the different kinds of atoms were made and repeated in such a way that the first 25 SRO parameters calculated on the basis of the atomic arrangements fit the experimentally determined values. The atoms on a boundary were connected to the other side of the boundary by using periodic boundary conditions. The CPU time was 60 s.

Figs. 9(*a*) and (*b*) show the distributions of Mn atoms on the 10 × 10 × 10 unit cells simulated in this way for the ideal perfect disordered structure and for the observed SRO structure, respectively. In the figures only Mn atoms are represented, by circles, and they are linked together by solid lines if they are first and second neighbours in the f.c.c. lattice. Fig. 9(*c*) shows the Mn atom arrangement in the ordered state which is stable below 693 K with the Ni_4Mo type structure. In this structure Mn atoms are arranged in a body-centred tetragonal lattice with parameters $a_{tet} = \sqrt{10}a_{cub}/2$ and $c_{tet} = a_{cub}$. Long Mn atom chains ordered along the tetragonal c axis, corresponding to the second-neighbour [100] direction of the f.c.c. lattice, are formed as seen in the figure.

Comparisons of these three structures show that the probability of finding Mn atoms which adjoin each other with a nearest-neighbour relation is very high in the disordered structure. Such Mn chains do not exist in the ordered phase. On the other hand, Mn chains with a noticeable length along the second-neighbour [100] direction cannot be found in the disordered structure. It is clear from the figures that the Mn atom arrangement in the SRO structure, Fig. 9(*b*), lies somewhere between the two extreme cases. In the SRO structure the tendency of the Mn atoms to line up along the [100] direction still remains, while the number of adjoining Mn atoms is not negligible. One also notices that almost all the Mn atoms are linked with either first- or second-neighbour relations and form an irregular Mn network. This is quite different from the local atomic arrangement predicted by FEG in which Mn atom chains with different lengths exist as well as other isolated complex Mn clusters in this disordered alloy. It seems likely, however, that the probability of finding such isolated clusters is very rare. It seems possible to characterize the structure of the SRO state by the existence of such an irregular three-dimensional Mn network in a f.c.c. lattice. This would be very strongly

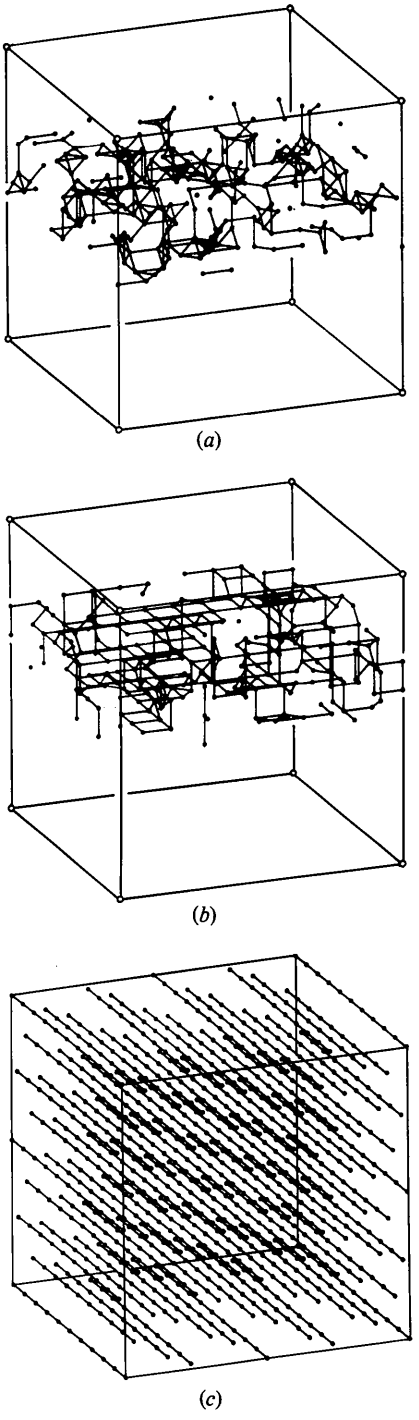

Fig. 9. Three-dimensional distributions of Mn atoms simulated on 10 × 10 × 10 f.c.c. unit cells; (*a*) for ideal perfect disordered state, (*b*) for the observed SRO state of Au_4Mn alloy, and (*c*) for the ordered state of the Ni_4Mo-type structure. The Mn atoms which are in first- and second-neighbour relations are linked together by a solid line. The SRO structure is characterized by an irregular three-dimensional Mn network linked by linear chain segments along the [100] directions and also by nearest-neighbour relations.

related to its ferromagnetic properties, as will be discussed in the next section.

4. Ferromagnet in the SRO state

Fig. 10 shows Ido's (1973) measurements of the magnetization M_s and inverse susceptibility $1/\chi_g$ *vs* temperature T for the ordered as well as the SRO structure of the present Au_4Mn alloy sample. The temperature dependences of M_s and $1/\chi_g$ of the ordered state show the well known behaviour of ferromagnetic phase transitions. The Curie temperature $T = 373$ K is

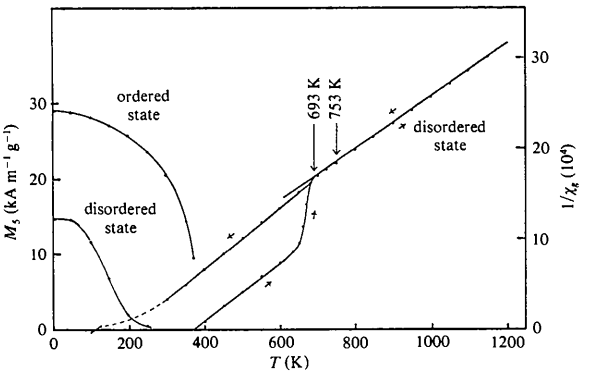

Fig. 10. The magnetization M_s and inverse susceptibility $1/\chi_g$ for the ordered and disordered Au_4Mn as a function of temperature T in the magnetic field of 1·43 MA m^{-1}.

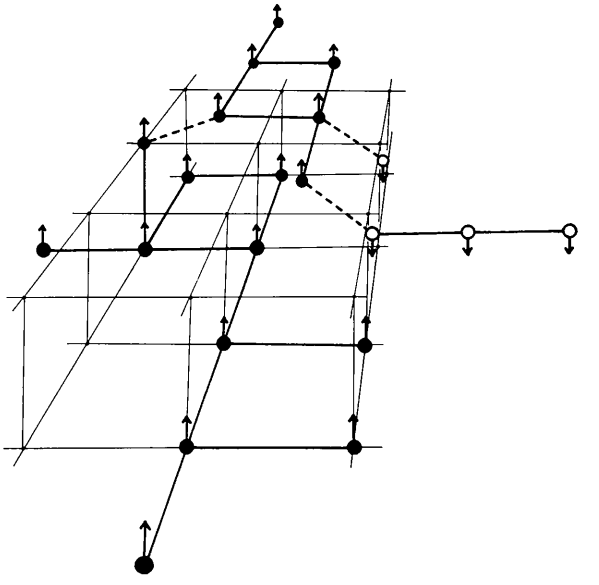

Fig. 11. A possible spin configuration with antiferromagnetic coupling in the SRO state of Au_4Mn alloy. The spin directions are assigned for the Mn atom in the second- and third-neighbour relations to have a ferromagnetic arrangement and for those in the first-neighbour relation to have an antiferromagnetic arrangement. The first neighbours are linked by dashed lines and the second neighbours by solid lines.

well defined in both plots. The magnetization in the SRO state could only be measured under strong magnetic field. Its magnitude is about half the magnitude of M_s in the ordered state at low temperatures. It decreases gradually to zero near 200 K. The Curie temperature, however, is not so well defined as in the ordered state. The inverse susceptibility, $1/\chi_g$, of the SRO state obeys the Curie–Weiss law very nicely with almost the same slope as the ordered state except in a narrow temperature range near 200 K. This indicates that the Mn atom has the same effective number of Bohr magnetons in the SRO state as in the ordered state; observed values of $p_{\text{eff}}(\mu_B)$ are $4{\cdot}5 \pm 0{\cdot}2$ and $4{\cdot}8 \pm 0{\cdot}2$ for the SRO and the ordered state, respectively. This is typical magnetic behaviour of random spin distribution systems if a concentration gradient of spin density does exist. The fact that the magnetization does not saturate easily except in the presence of a strong magnetic field indicates the presence of some irregular arrangement of small ferromagnetic domains owing to the presence of antiferromagnetic coupling in this system. It may be said that the three-dimensional irregular Mn atom network connected by the first- and second-neighbour relations in the f.c.c. lattice, as obtained by computer simulation, is just what one would expect from a random spin system with a concentration gradient, as it is reasonable to assume that the Mn pairs connected by the nearest-neighbour relation have antiferromagnetic coupling, while those with second- and third-neighbour relations have ferromagnetic coupling. In Fig. 11 one part of the irregular Mn network is reproduced in order to visualize more clearly such spin arrangements. Although the upper part of a Mn chain is connected with the lower part in an antiphase relation where the chains are displaced by half a unit cell, they are all assigned as arranged with the same spin. We see clearly the existence of opposite spin connections with nearest-neighbour relations in this complex structure which does not exist in the ordered structure of the Au_4Mn alloy. Such a spin arrangement is understood to reduce the saturation magnetization of the SRO state, compared with that of the ordered state. It, therefore, follows that the ferromagnetic state cannot be obtained for the ideally perfect disordered alloy, as shown in Fig. 9(*a*).

It seems very likely that the relationship between the peculiar magnetic property and the structure of the Mn atom arrangements in the SRO state has been solved by the present study. In previous studies this magnetic property has been considered simply to be attributed to the existence of either small Mn clusters of microdomains with ordered Mn arrangements.

It would be interesting to do similar structural studies on more dilute alloys in connection with their magnetic properties.

The authors wish to thank Professor M. Koiwa of the Research Institute for Iron, Steel and Other Metals, Tohoku University for the use of his simulation program. Special thanks go to Dr T. Shanmugan of the School of Physics, University of Melbourne for the careful reading of our manuscripts. Thanks are also due to Mr H. Yamamoto of the HIX Laboratory, Nagoya University, for experimentation. All the calculations in the present study were carried out on the Facom-M200 computer of Nagoya University Computation Center.

References

BORIE, B. & SPARKS, C. J. (1971). *Acta Cryst.* A**27**, 198–201.

CLAPP, P. C. & MOSS, S. C. (1966). *Phys. Rev.* **142**, 418–427.

CLAPP, P. C. & MOSS, S. C. (1968*a*). *Phys. Rev.* **171**, 754–763.

CLAPP, P. C. & MOSS, S. C. (1968*b*). *Phys. Rev.* **171**, 764–777.

FÜRNROHR, P., EPPERSON, J. E. & GEROLD, V. (1980). *Z. Metallkd.* **71**, 403–409.

GEHLEN, P. C. & COHEN, J. B. (1965). *Phys. Rev.* **139**, A844–A855.

HAYAKAWA, M., BARDHAN, P. & COHEN, J. B. (1975). *J. Appl. Cryst.* **8**, 87–95.

HIRABAYASHI, M., KOIWA, M., YAMAGUCHI, S. & KAMATA, K. (1978). *J. Phys. Soc. Jpn*, **45**, 1591–1598.

IDO, J. (1973). D.Eng. thesis. Nagaya Univ., Chikusaku, Nagoya, Japan.

KÖSTER, W. & HUMMEL, R. E. (1964). *Z. Metallkd.* **55**, 175–179.

NAKASHIMA, T., MIZUNO, S., IDO, T., SATO, K., MITANI, S. & ADACHI, K. (1977). *J. Phys. Soc. Jpn*, **43**, 1870–1878.

TIBBALLS, J. E. (1974). PhD thesis. Univ. of Melbourne, Parkville, Australia.

WILLIAMS, R. O. (1976). Report ORNL-5140. Oak Ridge National Laboratory, Tennessee.